Corrosion Science 74 (2013) 387–395

Contents lists available at SciVerse ScienceDirect

Corrosion Science

journal homepage: www.elsevier.com/locate/corsci

Corrosion behavior of Cu–Al–Be shape memory alloys with different compositions and microstructures

S. Montecinos [a,b,*], S. Simison [b,c]

[a] Instituto de Física de Materiales Tandil-IFIMAT, Facultad de Ciencias Exactas, Universidad Nacional del Centro de la Provincia de Buenos Aires, Pinto 399, 7000 Tandil, Argentina
[b] CONICET, Av. Rivadavia 1917, CABA, Argentina
[c] INTEMA, Facultad de Ingeniería, Universidad Nacional de Mar del Plata, Juan B. Justo 4302, 7600 Mar del Plata, Argentina

ARTICLE INFO

Article history:
Received 20 March 2013
Accepted 15 May 2013
Available online 24 May 2013

Keywords:
A. Alloy
B. Polarization
B. Potentiostatic
B. Weight loss
C. De-alloying
C. Passive films

ABSTRACT

The corrosion behavior of Cu–Al–Be shape memory alloys with different microstructures and Be content in a 3.5% NaCl solution was studied by weight loss, cyclic anodic polarization and chronoamperometric measurements. The beryllium has a beneficial effect in β alloys. A pitting potential of −100 mV/SCE was found by anodic polarization tests for all the studied alloys, corresponding to the formation of pits produced by severe dealuminization. Samples with precipitates were more susceptible to pit formation. The corrosion behavior is strongly affected by the alloy microstructural conditions, and the β samples present higher pitting resistance and repassivation ability.

1. Introduction

Previous investigations on Cu–(11.4–11.8 wt.%)Al shape memory alloys with the addition of small quantities of beryllium have shown that they exhibit the pseudoelastic effect at room temperature, due to the martensitic transformation from the β phase to 18R martensite [1–5]. An important lowering of the martensitic transformation critical temperature is obtained with the addition of small amounts of beryllium, −89.3 °C each 0.1 wt.%Be [2]. This decrease of the critical temperature enlarges the temperature range at which the shape memory effect is operative. There is an interest in the possible effect of small changes in the Be content on the corrosion behavior of the Cu–Al–Be shape memory alloys. The pseudoelastic effect is produced by the application of mechanical stress and when the load is removed, a hysteretic loop is formed and an almost complete recuperation of the strain could be obtained. The thermomechanical properties of Cu–Al–Be alloys have been studied [1,3–6], and their use is highly promising for applications as passive dampers of seismic energy in buildings and in bridges [4,7]. When these alloys are submitted to heat treatments like a slow cooling from high temperature or an isothermal heating, the formation of precipitates can be produced [8,9], and their presence can affect their shape memory properties [10].

Regarding the corrosion behavior of Cu–Al–Be alloys in chloride media, only studies at open circuit potential have been reported. In previous works we have studied the corrosion products formed on Cu–Al–Be alloys when they are immersed in a 3.5% NaCl solution up to 40 days, their evolution with the time and the influence of the microstructure on those products [11,12]. Chloride environment produces a dealuminization attack, resulting in a loss of aluminum from the alloy. This type of attack has been also reported by other authors for Cu–Al and Cu–Al–X alloys in chloride media [13,14]. However, the microstructure of the alloy is determinant on its corrosion resistance, and the formation of the corrosion products is affected by the aluminum content of each phase. For samples with γ_2 precipitates, the aluminum rich phase, the preferential dissolution of them occurs, which seems to protect the matrix from dealloying [11].

The aim of this work was to study the corrosion behavior of Cu–Al–Be shape memory alloys with different microstructures and Be content in a 3.5% NaCl solution in view of its application as seismic damper in bridges. The corrosion behavior was characterized by weight loss, cyclic anodic potentiodynamic polarization and chronoamperometric measurements. The effect of the beryllium was analyzed comparing samples with single β phase of two alloys: Cu–11.41Al–0.50Be (wt.%) (A1) and Cu–11.40Al–0.55Be (wt.%) (A2). The influence of the microstructure was studied in samples of alloy A2.

* Corresponding author at: Instituto de Física de Materiales Tandil-IFIMAT, Facultad de Ciencias Exactas, Universidad Nacional del Centro de la Provincia de Buenos Aires, Pinto 399, 7000 Tandil, Argentina. Tel.: +54 (0) 249 4439670; fax: +54 (0) 249 4439679.
E-mail address: dmonteci@exa.unicen.edu.ar (S. Montecinos).

0010-938X/$ - see front matter © 2013 Elsevier Ltd. All rights reserved.
http://dx.doi.org/10.1016/j.corsci.2013.05.012

2. Experimental procedure

Two commercial polycrystalline alloys were used in the present work: Cu–11.41Al–0.50Be (wt.%) (A1) and Cu–11.40Al–0.55Be (wt.%) (A2). They were provided by Trefimetaux S.A. Their chemical composition was determined by atomic absorption spectrophotometry. Samples with three different microstructures were studied, and they were obtained through the following heat treatments:

(a) Single β phase microstructure (Fig. 1a): The samples were kept during 5 min at 800 °C, in the β field, and water quenched at room temperature.

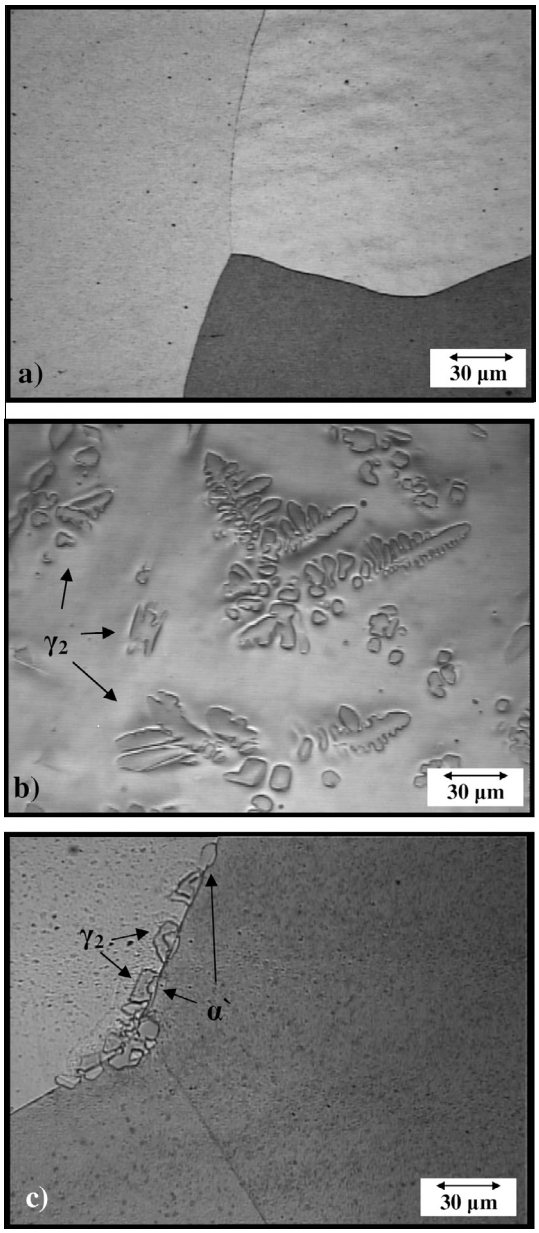

Fig. 1. Micrographs of samples with different microstructures obtained by optical microscopy: Single β phase (a); (β + γ_2) microstructure (b); and β + (α′ + γ_2) microstructure (c).

(b) (β + γ_2) microstructure (Fig. 1b): Precipitation of dendritic pro-eutectoid γ_2 phase was generated by slow cooling at around 1.3 °C/min from 800 °C to 535 °C, followed by water quenching at room temperature. A detailed description of the γ_2 phase formation is given in [8].

(c) β+(α′ + γ_2) microstructure (Fig. 1c): Precipitation of the eutectoid (α′ + γ_2) was generated by an isothermal aging treatment at 504 °C, followed by water quenching at room temperature. A detailed description of the eutectoid formation is given in [9].

The micrographs presented in Fig. 1 were obtained by optical microscopy. The samples were previously electropolished in a saturated solution of chromium trioxide in phosphoric acid at around 4 V, and immersed for a few seconds in a solution of ferric chloride in order to reveal the microstructural details.

For all the heat treatments, the temperature was monitored using a chromel–alumel thermocouple. The volume fraction (fv) of precipitates in the specimens was estimated from optical micrographs as the relative area occupied by them with respect to the total area using the software Image Tool 3.0. In the (β + γ_2) microstructure, a fv of 15 ± 2% of γ_2 phase was estimated, and they were almost homogeneously distributed on the samples. In the β + (α′ + γ_2) microstructure, a fv around 1–2% of each precipitated phase was estimated, and they were located mainly in the area of grain boundaries and at the edges of the samples. The samples were smoothed with 240, 600 and 1000 grit emery paper, and then rinsed with distilled water, sprayed with ethanol and dried with hot air.

For corrosion tests, specimens were immersed in a 3.5% NaCl solution adjusted to pH 8.0 with borate–boric acid buffer at room temperature (20 ± 2 °C) and bubbled with air.

The weight loss tests were carried out using disk coupons from the alloy A2, with β and (β + γ_2) microstructures, and having dimensions of 15 mm diameter and ~1.8 mm thick. Prior to the tests, each coupon was measured and weighted. For each microstructure, one sample was immersed during 18 days, and two of them were immersed during 45 and 60 days. Once the test was finished for each immersion time, the samples were extracted, and the corrosion products were removed using a soft brush and a 10% HCl solution. After that, they were neutralized with a saturated Na_2CO_3 solution, and then rinsed with distilled water, sprayed with ethanol and dried with hot air. This procedure to remove the corrosion products and surface neutralization has been previously used [15]. The cleaned and dried samples were weighted using a balance with a resolution within 0.1 mg.

The electrochemical measurements were performed in a conventional three electrode cell, using a potentiostat (Voltalab PGZ 402) and a cell of 150 mL volume. A platinum wire with an exposed area of around 2.5 cm^2 and a Saturated Calomel Electrode (SCE) were used as counter and reference electrodes, respectively. The working electrodes were prepared with cylindrical samples of 5.4 mm diameter which were embedding in Teflon holders to expose a circular area of around 0.23 cm^2 to the electrolyte. After 24 h of immersion at open circuit potential, cyclic anodic polarization curves were carried out, starting at the open circuit potential (E_{OCP}) for each sample at a sweep rate of 1 mV s^{-1}. Potential was reversed at an arbitrary chosen current density of 400 μA/cm^2. Potentiostatic current–time tests were conducted after 30 min of immersion at E_{OCP}, maintaining the potential for 1 h from −300 mV/SCE with 0.025 V increments in the anodic direction. Between each experiment, samples were kept 1 h at −800 mV/SCE.

The surface morphology of the samples after corrosion tests was examined using an Olympus PMG3 optical microscope (OM) and a JEOL JSM-6460LV scanning electron microscope (SEM). Energy dispersive X-ray spectroscopy (EDX) analysis under SEM was

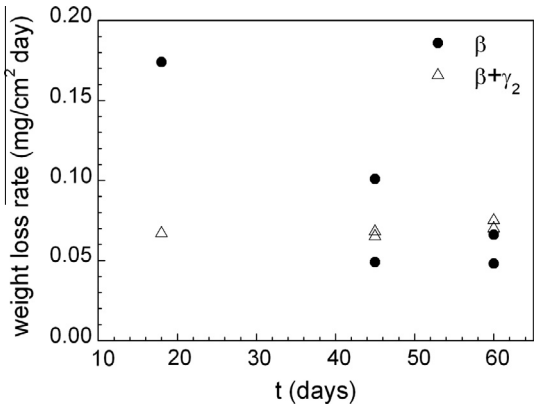

Fig. 2. Variation of weight loss rate of β-A2 and (β + γ_2)-A2 samples with exposure time.

employed to obtain an estimation of the surface composition of different regions of the samples. Their variability was obtained as the standard deviation of at least three experimental measurements.

3. Results

3.1. Weight loss measurements

The weight loss values of A2 samples with β and (β + γ_2) microstructures are shown in Fig. 2. An almost constant value of weight loss rate of around 0.07 mg/cm^2 day was measured for the (β + γ_2) samples, while values decreased with the exposure time in the case of β samples. This behavior has been described for other Cu–Al–X alloys in a chloride environment, reporting rates in the range of 0.04–0.07 mg/cm^2 day after around 20 days of immersion [16–18]. For 60 days exposure time, the differences of rates between both microstructures of the studied alloy turned small. Also, higher dispersion was obtained between different specimens of β samples. Figs. 3 and 4 show the corroded surfaces after 45 days of immersion in 3.5% NaCl. In both microstructures, grains were revealed by the corrosion process. β samples presented corrosion localized in some regions (zone A in Fig. 3), whereas the (β + γ_2) microstructure exhibited the darkening of the precipitates, and the matrix seems to be only slightly corroded (Fig. 4). These results are in agreement with those reported in [11] for a similar alloy immersed in 3.5% NaCl for 40 days, where the corrosion in the single β phase microstructure after long exposure times is produced by the dealuminization of the matrix, with severe localized corrosion attack zones, while in the two-phases microstructure the dissolution of the precipitates occurs. The observations of the sample surfaces indicated that the corrosion process is more homogeneously distributed in the (β + γ_2) microstructure, which is consistent to an almost constant value of weight loss rate. On the other hand, the corrosion process in the samples with single β phase is more localized and the affected area is less reproducible with higher dispersion in the weight loss rates.

3.2. Electrochemical tests

To study the influence of the microstructure on the electrochemical behavior of Cu–Al–Be alloys, cyclic anodic potentiodynamic polarization and chronoamperometric measurements were performed on at least two samples of each microstructure of A2.

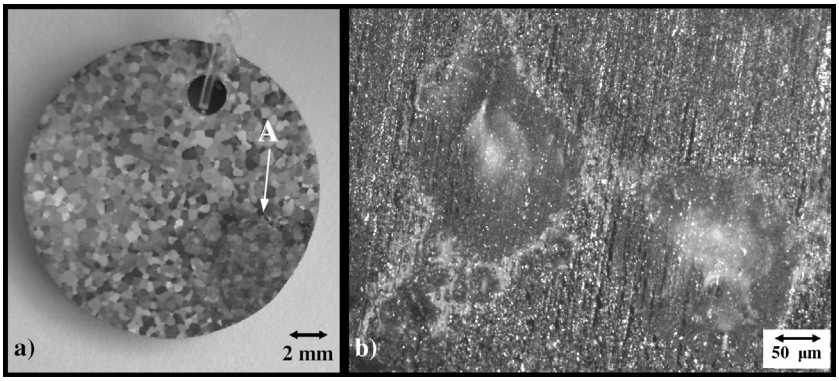

Fig. 3. β Sample after 45 days of immersion in 3.5% NaCl: (a) Surface of the specimen, and (b) optical micrograph of a zone with severe localized corrosion (zone A in a).

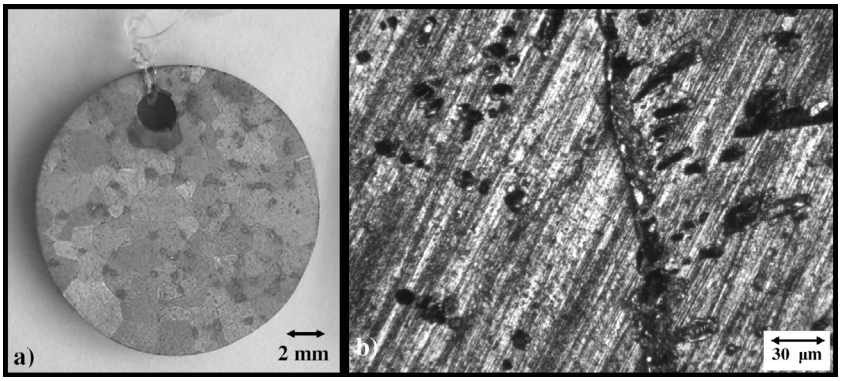

Fig. 4. (β + γ_2) Sample after 45 days of immersion in 3.5% NaCl: (a) Surface of the specimen and (b) optical micrograph of a representative zone.

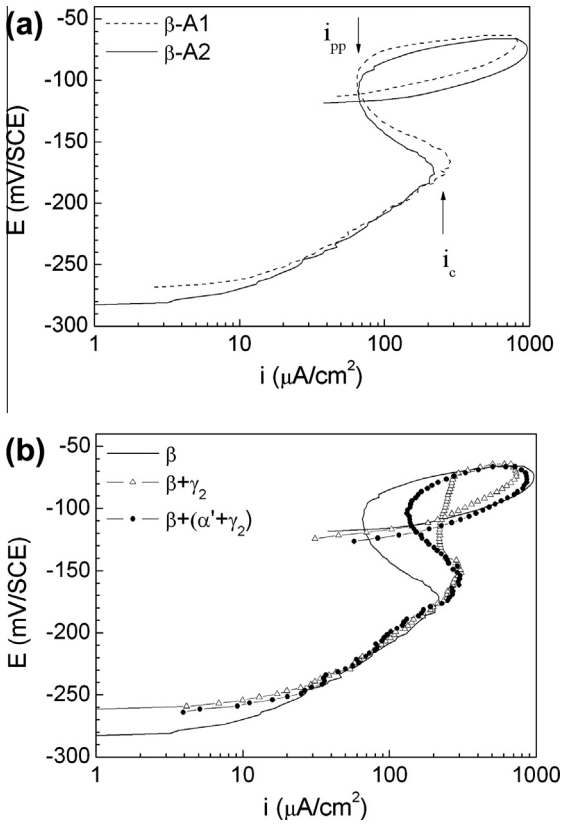

Fig. 5. Anodic polarization curves for: (a) β-A1 and β-A2, and (b) A2 with different microstructures in 3.5% NaCl solution.

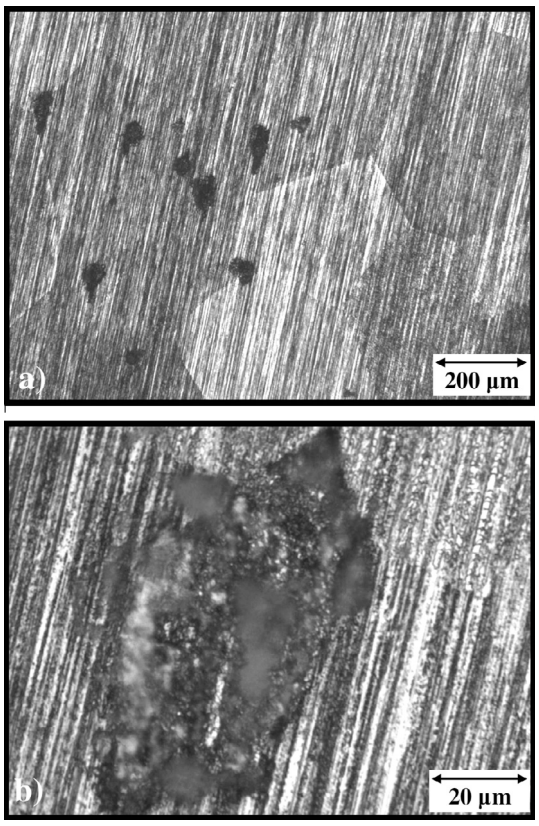

Fig. 6. β-A2 Sample after the anodic polarization test in 3.5% NaCl. (b) is a magnified micrograph of (a) (OM).

The influence of slight differences of beryllium was analyzed comparing samples with single β phase of both alloys.

3.2.1. Anodic potentiodynamic polarization

Representative curves of each type of sample are shown in Fig. 5. The first almost linear part corresponds to the apparent Tafel region and a critical current density (i_c) is reached, then the electrode presents a tendency to passivate with a decrease in the current until a pseudo-passive current density (i_{pp}). The term pseudo-passive is used for the studied alloy, due to the decrease in current is not as significant as in other passive materials. After that, the current rises again with the increase of the potential until the scanning is reversed. This is the typical anodic behavior for dissolution of copper and copper alloys in chloride solutions [19]. The potential at which the repassivation occurs is in the range −110 mV/SCE to −120 mV/SCE for both alloys and microstructures. The curves of the single β phase microstructure for both alloys are very similar (Fig. 5a) and no significant effect of beryllium was observed on the anodic curves. However, the corrosion behavior is strongly affected by the alloy microstructural conditions (Fig. 5b), as has been reported previously [11]. The average values of i_c, i_{pp},

Table 1
Parameters obtained from anodic polarization curves. The scatter bands were obtained as the standard deviation of at least three experimental measurements.

Alloy	Microstructure	i_c (μA/cm²)	i_{pp} (μA/cm²)	β_a (mV/decade)	E_{OCP} (mV/SCE)
A1	β	191 ± 30	46 ± 10	85 ± 7	−280 ± 8
A2	β	208 ± 42	54 ± 8	80 ± 1	−286 ± 1
	(β + γ2)	335 ± 28	218 ± 1	88 ± 1	−269 ± 6
	β + (α' + γ2)	244 ± 33	113 ± 17	85 ± 6	−250 ± 18

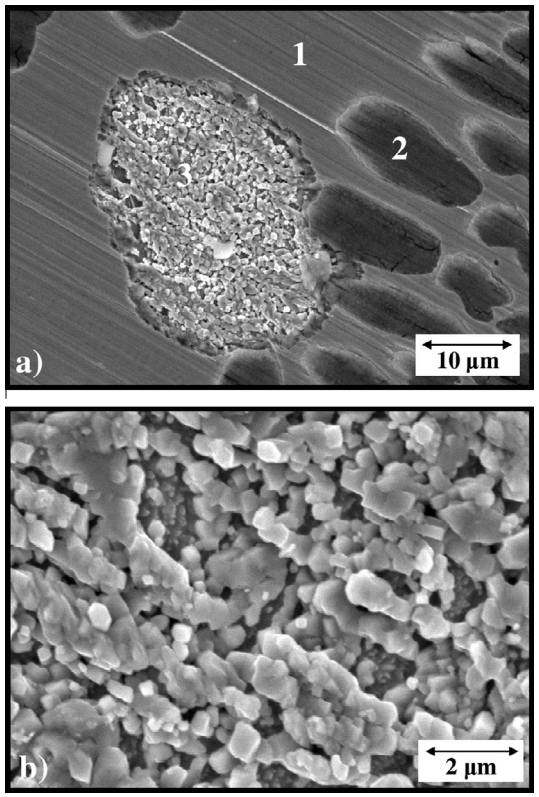

Fig. 7. (β + γ2) Sample after the anodic polarization test in 3.5% NaCl. (b) is a magnified micrograph of zone 3 (SEM).

the Tafel anodic slope (β_a), and E_{OCP} obtained from at least three curves of each microstructure of A2 and of β-A1 samples are presented in Table 1. The slight differences between β-A1 and β-A2 samples are within the error range of the experimental data.

The anodic Tafel slopes were found to be around 0.08 V/decade for the β microstructure, which is close to the theoretical and experimental value of 0.06 V/decade for copper in chloride media at room temperature [13,20]. It has been established that Cu dissolves to $CuCl_2^-$ species and this process is determined by the rate of diffusion of soluble species from the electrode surface into bulk solution. The initial corrosion product of copper is cuprous chloride, CuCl [20]. It was proposed that the cuprous chloride, which is only slightly soluble in dilute sodium chloride, reacts to produce cuprous oxide (cuprite) which was the main constituent of thick scales. In Cu–Al alloys, it can be expected that aluminum dissolution occurs in addition to the dissolution of copper [13]. According to Chun et al. [21], the CuCl salt layer formed on Cu–Al alloys may be incorporated with the Al salt films such as AlCl and $Al(OH)_2Cl$. Apparent Tafel slopes in the range of 0.058–0.076 V/decade have been obtained by other authors for Cu–Al alloys in chloride media [13,19,22,23], suggesting that the same rate-determining step as in pure copper is operating in Cu–Al alloys. The samples with single β

Table 2
EDX analysis of (β + γ_2) sample before and after the anodic polarization test in 3.5% NaCl. The scatter bands were obtained as the standard deviation of at least three experimental measurements.

Element	Mass concentration (wt.%)				
	Before		After		
	Matrix	γ_2 phase	Zone 1	Zone 2	Zone 3
Cu	87.9 ± 0.1	83.7 ± 0.2	87.6	45.3	96.0
Al	12.0 ± 0.1	16.3 ± 0.2	11.3	24.7	1.1
O			0.9	28.8	2.6
Cl			0.2	1.2	0.3

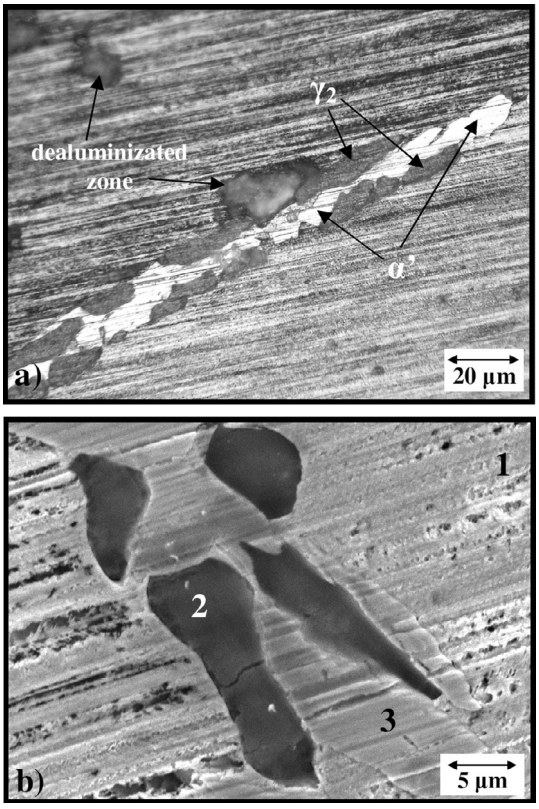

Fig. 8. β + (α′ + γ_2) Sample after the anodic polarization test in 3.5% NaCl: OM (a) and SEM (b).

Table 3
EDX analysis of β + (α′ + γ_2) sample before and after the anodic polarization test in 3.5% NaCl.

Element	Mass concentration (wt.%)					
	Before [12]			After		
	Matrix	γ_2 phase	α′ phase	Zone 1	Zone 2	Zone 3
Cu	85.2 ± 0.3	81.7 ± 0.3	88.4 ± 0.7	88.5	23.0	90.3
Al	14.8 ± 0.3	18.3 ± 0.3	11.6 ± 0.7	10.4	34.7	8.7
O				0.9	41.1	0.8
Cl				0.2	1.2	0.2

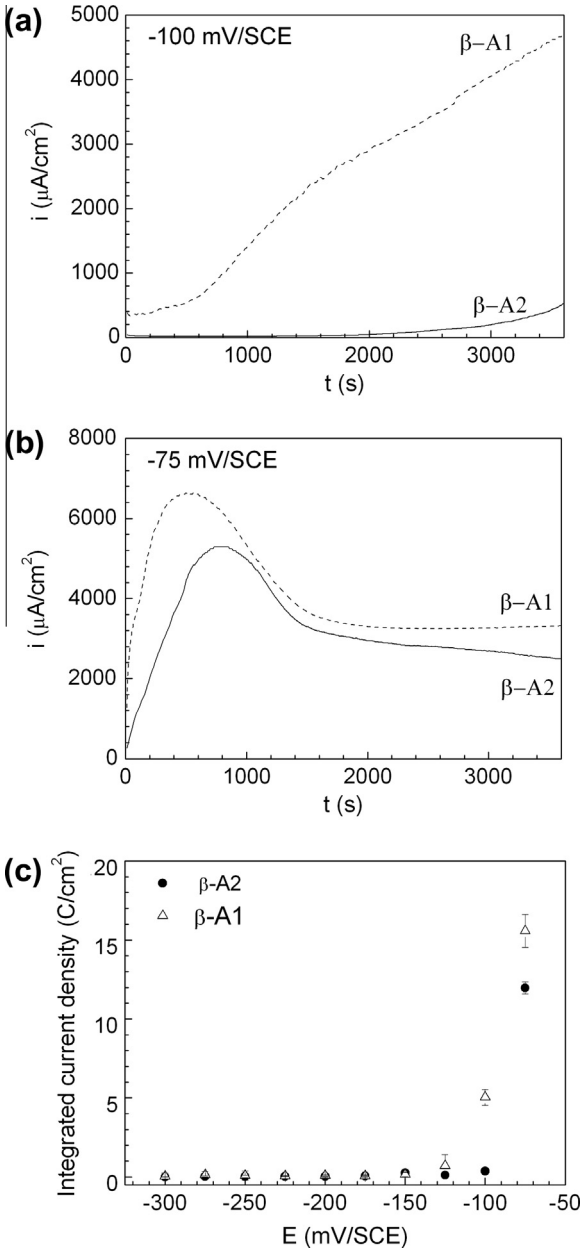

Fig. 9. Chronoamperometric curves at −100 mV/SCE (a) and −75 mV/SCE (b) for β-A1and β-A2 samples. (c) Variation of the integrated current density reached after 1 h of polarization at different potential steps.

phase tend to passivate at lower potentials and they also present lower E_{OCP}. Those samples also show lower current densities respect to the specimens with precipitates. The highest current density was obtained for the ($\beta + \gamma_2$) microstructure. These results suggest that the presence of precipitates worsens the passivation behavior of Cu–Al–Be alloys.

To understand the different corrosion processes occurring during the anodic polarization tests in the three microstructures, surface morphologies of specimens were analyzed with OM and SEM with EDX after the tests. Fig. 6 shows the surface of a β-A2 sample. Numerous pits were observed on the surface of the samples. These regions correspond to small zones where the corrosion attack was more severe due to aluminum preferential dissolution. This attack morphology is found to be different to that observed in the same alloy after long times of immersion at open circuit potential [11], where the dealuminized areas were concentrated in one or two spots on the sample surface.

Fig. 7 shows the surface of a ($\beta + \gamma_2$) sample after the anodic polarization test. The EDX analysis results from different zones before and after the tests are given in Table 2. After the tests, the matrix was slightly impoverished in Al and contains some corrosion products (zone 1). The precipitates present a surface film rich in O and Al, which would correspond to Al_2O_3 [11], and small quantities of Cl (zone 2). Some pits produced by a severe dealuminization were observed on the matrix (zone 3), containing a porous product with copper content as high as 96 wt.%. In other zones of the sample, the Al_2O_3 film could not be observed on some precipitates, and also a porous product rich in copper was observed.

Fig. 8 shows the surface of a $\beta + (\alpha' + \gamma_2)$ sample after the anodic polarization test. The γ_2 precipitates are darker, while α' phase is brighter respect to the matrix (Fig. 8a). Some pits produced by dealuminization were also observed in the samples (Fig. 8a). The EDX analysis results from different zones before and after the tests are given in Table 3. The compositions of the three phases in the freshly polished samples were obtained from reference [12], and the compositions of different zones of the samples correspond to the areas indicated in Fig. 8b. γ_2 precipitates are the aluminum rich phase and α' is the copper rich phase (Table 3). After the tests, the matrix and the γ_2 precipitates present a similar behavior to the ($\beta + \gamma_2$) sample: the matrix was slightly impoverished in Al (zone 1) and an Al_2O_3 film was formed on the precipitates (zone 2). α' phase was also impoverished in Al (zone 3).

3.2.2. Chronoamperometric measurements

For potentials lower than −125 mV/SCE, the current density remains almost constant with values smaller than 200 μA/cm^2 after 1 h in the β phase microstructure in both alloys. Representative current–time curves for the single β phase microstructure corresponding to both alloys at −100 mV/SCE and −75 mV/SCE are presented in Fig. 9. At −100 mV/SCE the current increases rapidly in A1, while it remains low in A2 (Fig. 9a). At −75 mV/SCE both alloys present a similar behavior, with higher current densities in A1 (Fig. 9b). The shape of the measured curves would be associated to the passivation of the dealloyed pits due to the copper accumulation [24]. The current density presents a large initial increase, reaching a maximum value of 6600 μA/cm^2 within 500 s in alloy A1, and 5300 μA/cm^2 within 800 s in A2. Then, it slowly decreases and a current density of around 3000 μA/cm^2 is finally reached after 1 h of polarization. The values of the integrated current density reached after 1 h of polarization at different potential steps for both alloys are presented in Fig. 9c. The errors were estimated as the standard deviation of the measurements. The lower currents of the alloy A2 respect to A1 for the same potential, suggest that the beryllium has beneficial effects: less amount of dissolved

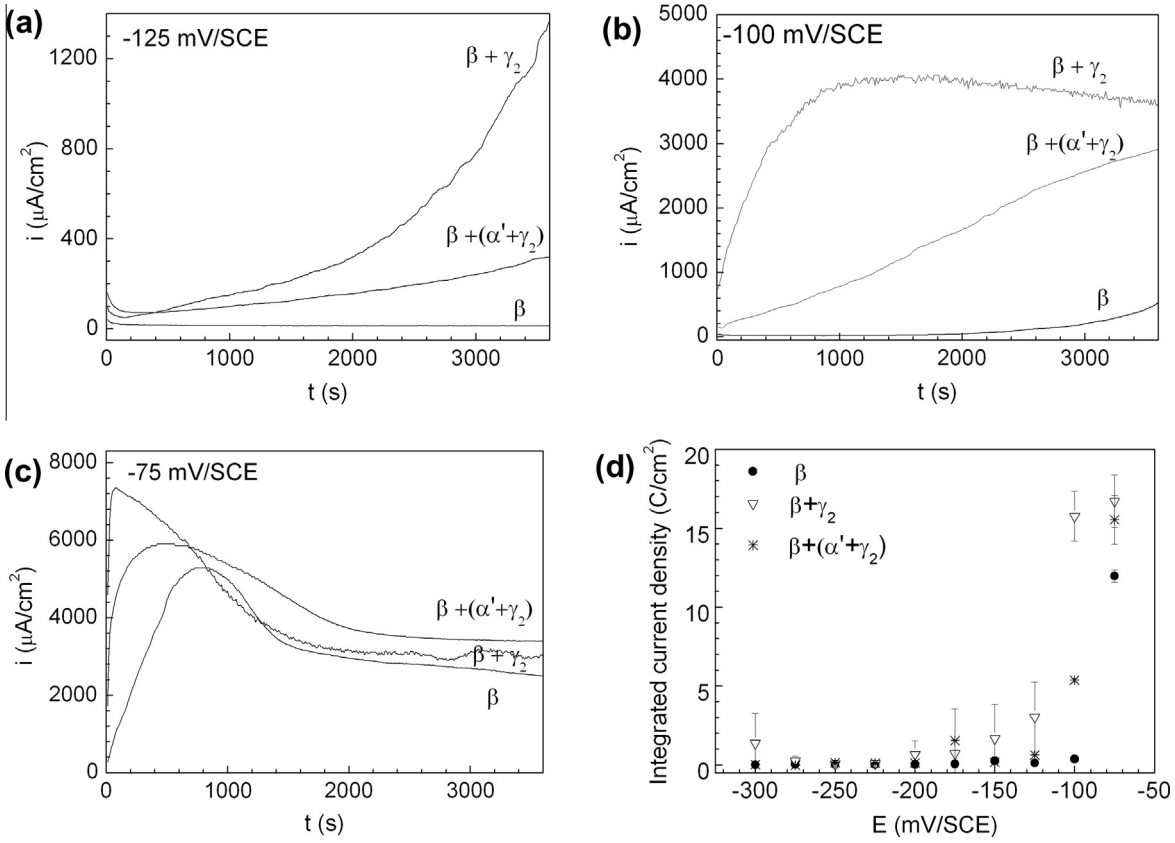

Fig. 10. Chronoamperometric curves at −125 mV/SCE (a), −100 mV/SCE (b), and −75 mV/SCE (c) for A2 samples with different microstructures. (d) Variation of the integrated current density reached after 1 h of polarization at different potential steps.

material is needed in order to repassivate the pits and also the pseudo-passive film seems to be more protective.

Significant differences can be observed in samples with the same beryllium content and different microstructures as shown in Fig. 10. At −125 mV/SCE, the current density remains almost constant in the β phase microstructure, while in β + (α′ + γ_2) samples it increases slightly, and in (β + γ_2) samples it increases up to 1366 μA/cm^2 (Fig. 10a). At −100 mV/SCE, (β + γ_2) samples reach a maximum current density of 4000 μA/cm^2 and then slightly decreases until 3600 μA/cm^2, while the current increases in the other microstructures reaching values of 2900 μA/cm^2 and 500 μA/cm^2 after 1 h immersion, for β + (α′ + γ_2) and β specimens, respectively (Fig. 10b). The passivation of the dealloyed pits occurs at −75 mV/SCE in all the samples, the current density reaches a maximum and then slightly decreases up to around 3000 μA/cm^2 (Fig. 10c). Higher currents are reached for the samples with precipitates respect to the specimens with single β phase, and this effect is more pronounced for (β + γ_2) samples, in agreement with the higher volume fraction of precipitates. A significant increase of the current density can be observed at −125 mV/SCE for (β + γ_2) samples, while it occurs at −75 mV/SCE for the specimens with single β phase. The integrated current density reached after 1 h of polarization at different potential steps for the three microstructures are presented in Fig. 10d. The errors were estimated as the standard deviation of the measurements. It can be seen that samples with single β phase keep pseudo-passivity at more anodic potentials. These results indicate that samples with precipitates were more susceptible to pit formation than the samples with single β phase.

Fig. 11 shows the surface of a β sample after 30 min immersion and 1 h of polarization at −100 mV/SCE, −800 mV/SCE and 10 min at −75 mV/SCE up to a current density of 3200 μA/cm^2. Extensive areas with a severe dealuminization were observed in the surface

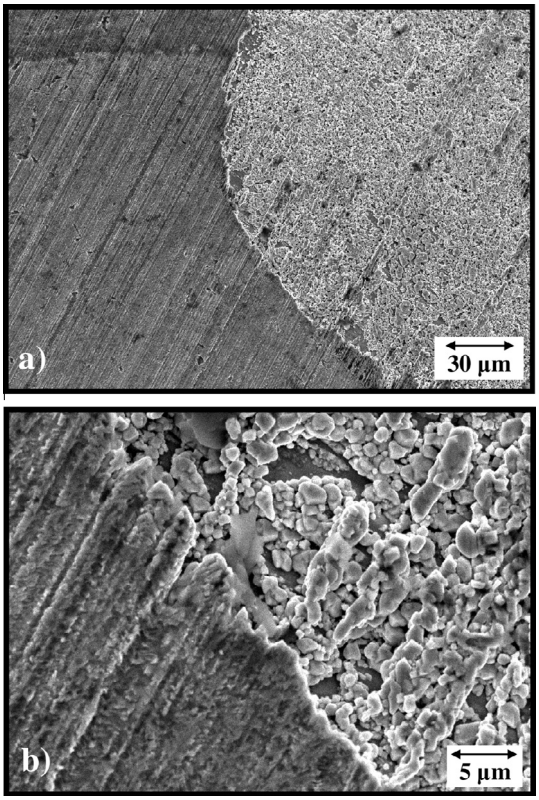

Fig. 11. β Sample after 30 min immersion and 1 h of polarization at −100 mV/SCE, −800 mV/SCE and 10 min at −75 mV/SCE up to a current density of 3200 μA/cm^2 (SEM). (b) is a magnified micrograph of (a).

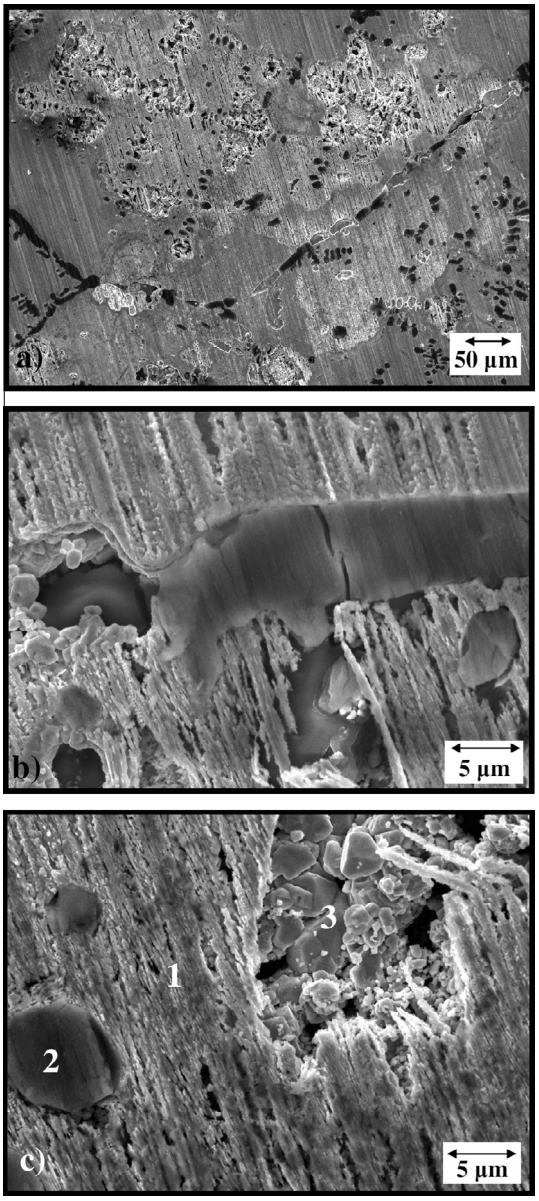

Fig. 12. (β + γ_2) Sample after 24 h immersion and 30 min of polarization at −100 mV/SCE up to a current of 3200 μA/cm^2 (SEM).

sample, showing in some of them a porous product with copper content as high as 95 wt.% (right side in Fig. 11b).

Fig. 12 shows the corroded surface of a (β + γ_2) sample after 24 h immersion and 30 min of polarization at −100 mV/SCE up to a current density of 3200 μA/cm^2. The EDX analysis results from the different zones indicated in Fig. 12c are given in Table 4. The matrix was impoverished in Al and contains some corrosion products based on O (zone 1). In some zones an Al_2O_3 film can be observed on the precipitates (zone 2), while this film is absent in other regions and particles of redeposited Cu could be observed inside them (zone 3).

4. Discussion

According to the apparent Tafel slopes obtained for the studied alloy, the same rate-determining step as in pure copper could be considered, where the major electrode process is anodic dissolution of copper to form the cuprous dichloride anion [20]. For the

Table 4
EDX analysis of ($\beta + \gamma_2$) sample before and after 24 h immersion and a potentiostatic step of 30 min at −100 mV/SCE in 3.5% NaCl. The scatter bands were obtained as the standard deviation of at least three experimental measurements.

Element	Mass concentration (wt.%)				
	Before		After		
	Matrix	γ_2 phase	Zone 1	Zone 2	Zone 3
Cu	87.9 ± 0.1	83.7 ± 0.2	85.1	22.9	99.2
Al	12.0 ± 0.1	16.3 ± 0.2	9.9	29.1	0.2
O			4.9	47.3	0.5
Cl			0.1	0.7	0.1

employed conditions, aerated solution and chloride media, this anodic reaction can be considered under mixed charge transfer and mass transport controlling kinetics at potentials close to E_{OCP} [20]. On the other hand, the primary cathodic process is the oxygen evolution, which would be under charge transfer control.

No significant effect of the beryllium content on the corrosion behavior was observed in the anodic polarization curves. However, lower current densities were reached in the alloy with higher beryllium content when it was maintained at −100 mV/SCE and −75 mV/SCE in the chronoamperometric measurements. It would suggest that the addition of small amounts of beryllium has a beneficial effect in the corrosion resistance of β phase alloys in a 3.5% NaCl solution. Kuo et al. [25] have found that small additions of beryllium, between 0.55 and 1.00 wt.%, in Cu–Al–Be alloys are effective to prevent the intergranular corrosion in 0.5 M H_2SO_4 solutions.

The influence of the microstructure on the corrosion behavior of A2 samples was studied. In samples with single β phase, the corrosion processes would occur mainly by the dissolution of both copper and aluminum [11,13]. After long times of immersion at E_{OCP}, the stable corrosion product formed on all the phases were $CuCl_2$ and a Cu_2O/CuO double layer [11], and the samples present some zones with severe localized dealuminization. This was confirmed by the chronoamperometric curves on the surface of samples maintained at potentials up to −75 mV/SCE, but the dealuminization is more significant, with some zones showing porous copper. After anodic polarization tests, some pits produced by dealuminization were observed on the surface of the samples. In ($\beta + \gamma_2$) samples, preferential dissolution of γ_2 phase occurs, a surface film of Al_2O_3 would form on the precipitates after short immersion times, but it is not detected after long exposure [11]. Instead of this film, copper rich layers and porous copper products are observed [11]. An analogous behavior was observed after the samples were maintained at potentials up to −100 mV/SCE (reaching a current density of 3200 μA/cm^2), the Al_2O_3 film was detected on some precipitates, while in others it was absent and Cu particles were observed in place of them. After anodic polarization tests, the Al_2O_3 surface film was detected on almost all the precipitates. It can be noted that when the dissolution is forced by an anodic overpotential, pits are produced in the matrix, unlike in open circuit potential tests [11], where only the precipitates are corroded. In $\beta + (\alpha' + \gamma_2)$ samples after anodic polarization tests: α′ phase was impoverished in Al, the matrix and the γ_2 phase exhibited a similar behavior to the ($\beta + \gamma_2$) samples, and pits were also observed on the matrix.

In the samples with precipitates, pits produced by dealuminization were formed mainly near the γ_2 phase, although, a few pits were also observed far from the precipitates. This result suggests that the regions surrounding those precipitates would act as preferential sites of nucleation for the pits. It could be associated to the deficiency in aluminum expectable near the γ_2 precipitates, which are rich in aluminum, and to the formation of the Al_2O_3 surface film on them. However, when the samples are immersed in chloride solutions at open circuit potential [11], pits do not form in the matrix.

During chronoamperometric tests, the formation of pits begins at around −125 mV/SCE in the samples with precipitates and at −100 mV/SCE in the samples with single β phase, and the passivation of the dealloyed pits occurs at −75 mV/SCE in all the specimens. In the samples with precipitates, the passivation would occur on the pits formed on the matrix and on those produced on the γ_2 precipitates, due to the accumulation of a product rich in copper. In a previous work [11] we found that the presence of γ_2 precipitates seems to protect the matrix from dealloying when the samples are immersed in a 3.5% NaCl solution at open circuit potential. However, at anodic potentials it is seen that the presence of those precipitates produces an increase of the current density and the matrix is also corroded.

The influence of beryllium and microstructure has been studied. More work has to be done in order to characterize the influence of corrosion on the mechanical response of these materials under cyclic loads aiming to assess the impact of the attack in the pseudoelastic capability. The obtained results also highlight the need to carry out in situ measurements of the corrosion processes occurring in different phases of Cu–Al–Be alloys, for example by atomic force microscopy observations.

5. Conclusions

The electrochemical behavior of Cu–Al–Be shape memory alloys with different microstructures was studied in a 3.5% NaCl solution. The effect of the beryllium was analyzed comparing samples with single β phase of two alloys: Cu–11.41Al–0.50Be (wt.%) (A1) and Cu–11.40Al–0.55Be (wt.%) (A2). The influence of the microstructure was studied by weight loss, cyclic anodic potentiodynamic polarization and chronoamperometric measurements in samples of A2 with different microstructures: Single β phase, ($\beta + \gamma_2$) and $\beta + (\alpha' + \gamma_2)$ samples. The following conclusions can be drawn:

(a) The addition of small amounts of beryllium has a beneficial effect in β phase alloys since lower current densities are needed in the alloy with higher beryllium content for the pseudo-passive film to be formed.
(b) By anodic polarization tests, a pitting potential of −100 mV/SCE was found for all the Cu–Al–Be alloys studied, corresponding to the formation of pits produced by severe dealuminization.
(c) From chronoamperometric tests, it was determined that samples with precipitates were more susceptible to pit formation than the samples with single β phase. The samples with single β phase present some zones with severe localized dealuminization, some of them showing porous copper. However, in ($\beta + \gamma_2$) samples, preferential corrosion of γ_2 phase occurs: a surface film of Al_2O_3 was detected on some precipitates, while in other it was absent and Cu particles were observed inside them.
(d) The corrosion behavior is strongly affected by the alloy microstructural conditions, and the samples with single β phase present a better behavior: higher pitting resistance and repassivation ability.

Acknowledgments

This work was supported by CONICET and Universidad Nacional de Mar del Plata. S.M. acknowledges ANPCYT and SECAT-UNCentro. The authors would also like to thank Lic. Mariela Desimone for her collaboration with the experimental measurements.

References

[1] B. Kaouache, S. Berveiller, K. Inal, A. Eberhardt, E. Patoor, Stress analysis of martensitic transformation in Cu–Al–Be polycrystalline and single-crystalline shape memory alloy, Mater. Sci. Eng. A378 (2004) 232–237.

[2] S. Belkahla, H. Flores Zuñiga, G. Guenin, Elaboration and characterization of new low temperature shape memory Cu–Al–Be alloys, Mater. Sci. Eng. A169 (1993) 119–124.

[3] S. Montecinos, A. Cuniberti, Thermomechanical behavior of a CuAlBe shape memory alloy, J. Alloys Compd. 457 (2008) 332–336.

[4] S. Montecinos, A. Cuniberti, Aplicación de aleaciones con memoria de forma CuAlBe en amortiguamiento pasivo de estructuras civiles, Rev. SAM 6 (3) (2009) 20–29.

[5] S. Montecinos, A. Cuniberti, A. Sepulveda, Grain size and pseudoelastic behaviour of a Cu–Al–Be alloy, Mater. Charact. 59 (2) (2008) 117–123.

[6] S. Kustov, J. Pons, E. Cesari, M. Morin, J. Van Humbeeck, Athermal stabilization of Cu–Al–Be β'_1 martensite due to plastic deformation and heat treatment, Mater. Sci. Eng. A373 (2004) 328–338.

[7] R. Desroches, B. Smith, Shape memory alloys in seismic resistant design and retrofit: a critical review of their potential and limitations, J. Earthquake Eng. 7 (3) (2003) 1–15.

[8] S. Montecinos, A. Cuniberti, M.L. Castro, R. Boeri, Phase transformation during continuous cooling of polycrystalline β-CuAlBe alloys, J. Alloys Compd. 467 (2009) 278–283.

[9] S. Montecinos, A. Cuniberti, M.L. Castro, Kinetics of isothermal decomposition in polycrystalline β CuAlBe alloys, Intermetallics 18 (2010) 36–41.

[10] A. Cuniberti, S. Montecinos, FC. Lovey, Effect of γ_2 phase precipitates on the martensitic transformation of a β-CuAlBe shape memory alloy, Intermetallics 17 (2009) 435–440.

[11] S. Montecinos, S.N. Simison, Influence of the microstructure on the corrosion behaviour of a shape memory Cu–Al–Be alloy in a marine environment, Appl. Surf. Sci. 257 (2011) 2737–2744.

[12] S. Montecinos, S.N. Simison, Study of the corrosion products formed on a multiphase CuAlBe alloy in a sodium chloride solution by micro-Raman and in situ AFM measurements, Appl. Surf. Sci. 257 (2011) 7732–7738.

[13] A.V. Benedetti, P.T.A. Sumodjo, K. Nobe, P.L. Cabot, W.G. Proud, Electrochemical studies of copper, copper–aluminium and copper–aluminium–silver alloys: Impedance results in 0.5 M NaCl, Electrochim. Acta 40 (16) (1995) 2657–2668.

[14] Z. Han, H. Zhao, Effect of β martensite transformation on dealuminification behaviour of Cu–9Al–2Mn alloy in a marine environment, Mater. Sci. Eng. A345 (2003) 8–13.

[15] M.B. Valcarce, S.R. de Sánchez, M. Vázquez, Localized attack of copper and brass in tap water: the effect of Pseudomonas, Corros. Sci. 47 (2005) 795–809.

[16] D.R. Ni, B.L. Xiao, Z.Y. Ma, Y.X. Qiao, Y.G. Zheng, Corrosion properties of friction-stir processed cast NiAl bronze, Corros. Sci. 52 (2010) 1610–1617.

[17] Chen. Rui-ping, Liang. Ze-qin, Zhang. Wei-wen, Zhang. Da-tong, Luo. Zong-qiang, Li. Yuan-yuan, Effect of heat treatment on microstructure and properties of hot-extruded nickel–aluminum bronze, Trans. Nonferrous Met. Soc. China 17 (2007) 1254–1258.

[18] B.G. Ateya, E.A. Ashour, S.M. Sayed, Corrosion of α-Al bronze in saline water, J. Electrochem. Soc. 141 (1) (1994) 71–78.

[19] M. Gojic, L. Vrsalovic, S. Kozuh, A. Kneissl, I. Anzel, S. Gudic, B. Kosec, M. Kliskic, Electrochemical and microstructural study of Cu–Al–Ni shape memory alloy, J. Alloys Compd. 509 (2011) 9782–9790.

[20] G. Kear, B.D. Barker, F.C. Walsh, Electrochemical corrosion of unalloyed copper in chloride media-a critical review, Corros. Sci. 46 (2004) 109–135.

[21] Y.-G. Chun, S.-I. Pyun, C.-H. Kim, Effect of aluminium content on the anodic behaviour of copper–aluminium alloys in 3.5 wt% NaCl solution, Mater. Lett. 20 (1994) 265–270.

[22] A.M. Alfantazi, T.M. Ahmed, D. Tromans, Corrosion behavior of copper alloys in chloride media, Mater. Des. 30 (2009) 2425–2430.

[23] G.C. Serra, A.V. Benedetti, R. Della Noce, Electrochemical behavior of Cu–9%Al–5%Ni–2%Mn alloy in chloride media, J. Braz. Chem. Soc. 21 (8) (2010) 1530–1536.

[24] J. Erlebacher, An atomistic description of dealloying. Porosity evolution, the critical potential, and rate-limiting behavior, J. Electrochem. Soc. 151 (10) (2004) C614–C626.

[25] H.H. Kuo, W.H. Wang, Y.F. Hsu, C.A. Huang, The corrosion behavior of Cu–Al and Cu–Al–Be shape memory alloys in 0.5 M H_2SO_4 solution, Corros. Sci. 48 (2006) 4352–4364.